IEEE Access
Multidisciplinary ⋮ Rapid Review ⋮ Open Access Journal

Received 9 August 2023, accepted 26 August 2023, date of publication 31 August 2023, date of current version 6 September 2023.

Digital Object Identifier 10.1109/ACCESS.2023.3310571

RESEARCH ARTICLE

Prediction Method for Propagation Path Loss Obstructed by Dielectric Material in the 920-MHz Band

NAOTAKE YAMAMOTO[1], (Member, IEEE), TAICHI SASAKI[1], (Member, IEEE), ATSUSHI YAMAMOTO[1], TETSUYA HISHIKAWA[1], AND JUN-ICHI TAKADA[2], (Senior Member, IEEE)

[1]Panasonic Corporation, Kadoma-shi, Osaka 571-8686, Japan
[2]Tokyo Institute of Technology, Meguro-ku, Tokyo 152-8550, Japan

Corresponding author: Naotake Yamamoto (yamamoto.naotake@jp.panasonic.com)

ABSTRACT This paper presents a simple calculation method for predicting the propagation path loss of a radio wave passing through a dielectric obstruction between a transmitter (Tx) and receiver (Rx). In this paper, the propagation characteristics of a radio that is obstructed by a concrete beam on a ceiling in a large indoor environment, such as those seen in factories and warehouses, are investigated. The radio frequency is the 920-MHz band, used for Internet-of-Things (IoT) wireless communications in Japan. The proposed calculation method is based on forbidden region (FR) theory, with the radius defined as 0.6 times that of the first Fresnel zone. In our proposed method, a three-wave model in the FR area at an obstructing object between Tx and Rx is considered for predicting the propagation path loss. The model consists of a wave propagating through the air, a wave penetrating the concrete beams, and a wave traveling inside the concrete ceiling. The path losses using the proposed calculation method are in good agreement with those of a Finite Difference Time Domain (FDTD) simulation and the measured data. We conclude that the proposed calculation method effectively predicts the path loss characteristics of radio waves obstructed by a dielectric material, such as a concrete beam on a concrete ceiling.

INDEX TERMS Indoor communication, Internet of Things (IoT), finite difference time domain (FDTD), prediction methods, radio propagation.

I. INTRODUCTION

With the recent growth of the Internet-of-Things (IoT) market, smart homes and smart factories are expected to be realized through machine-to-machine (M2M) and device-to-device (D2D) wireless communications [1], [2].

Indoor wireless communications encounter a number of obstructions between transmitter (Tx) and receiver (Rx) that create non-line-of-sight (NLoS) conditions. This makes the prediction of propagation path loss a key area of interest when designing systems. A number of prediction methods have therefore been studied to address this issue.

The associate editor coordinating the review of this manuscript and approving it for publication was Kegen Yu.

One well-known strategy for predicting the effects of obstructions along a propagation path loss is Fresnel zone theory [3], [4], which is obtained as an obstruction area ratio of the first Fresnel zone. There are also several theoretical approaches to predicting path loss, such as the knife-edge diffraction model (KEDM) [5], geometrical optics approximation (GO) [6], the geometrical theory of diffraction (GTD) [7], [8], uniform theory of diffraction (UTD) [9], [10], and slope-UTD [11], all of which have been used in terrestrial wireless communications.

In actual indoor situations, most obstructions, such as walls and pillars, are made of concrete. Radio waves are able to penetrate concrete objects, which have a relatively low dielectric constant [12]. However, in all of the abovementioned methods for predicting obstruction effects, the obstruction

is assumed to block all radio waves passing through the dielectric material.

Ray tracing is also widely used to predict propagation in indoor environments. This method takes account of waves passing through different materials. However, due to plane wave approximation, ray tracing calculations do not accurately predict the reflection, diffraction, or transmission coefficients of radio waves [13], [14]. The finite-difference time-domain (FDTD) method, which directly solves Maxwell's equations using a numerical approach, is increasingly being used for propagation prediction in indoor environments, assisted by recent advancements in high-performance computing [15], [16], [17], [18]. However, this method requires considerable computational resources to ensure calculation accuracy.

The purpose of this study is to propose a prediction method for propagation path loss that considers waves penetrating a dielectric material as an alternative to methods using sophisticated computer calculations, such as FDTD simulation. Our proposed prediction method takes advantage of forbidden region (FR) theory [19]. We evaluate here the propagation path loss in the 920-MHz band, used for IoT communication in Japan, caused by a concrete beam on a ceiling [20]. In the proposed method, we examine a three-wave model in the FR area at an obstructing object between Tx and Rx. The model consists of a wave propagating through the air, a wave penetrating the concrete beams, and a wave traveling inside the concrete ceiling. The propagation path loss is calculated using receiving power, which is obtained as the sum of the three waves with the amplitude obtained by the area ratio of the FR and the phase calculated using complex relative permittivity and traveling distance.

The structure of this paper is as follows. Chapter II describes the indoor scenario treated in this paper, and the path loss characteristics close to a concrete beam by FDTD simulation and by actual measurements. Chapter III gives the details of the proposed calculation method. In Chapter IV, the effectiveness of the proposed calculation method is verified by comparing with FDTD simulation results and measured data. In Chapter V, the path loss predictions are performed using the structural and material conditions of the concrete beam, assuming its application to real-world situations. Chapter VI concludes this study, lays out the limitation of this method, and suggests future work.

Table 1 summarizes the main abbreviations and symbols used in this paper.

TABLE 1. Abbreviations and symbols used in this paper.

Abbreviation	Definition
LoS	Line-of-sight
NLoS	Non-line-of-sight
FDTD	Finite Difference Time Domain
Tx	Transmitter
Rx	Receiver
FR	Forbidden region

Symbol	Definition
L	Path loss
$L_{concrete}$	Transmission loss through the concrete beam
h	Height of Tx and Rx antenna with respect to the bottom of the beam
d	Distance between Tx and Rx antenna
α	Path loss exponent
β	Path loss when distance between Tx and Rx antenna is 1 m ($d = 1$)
β_0	Free space path loss when distance between Tx and Rx antenna is 1 m ($d = 1$)
β_{ex}	Excess loss ($\beta - \beta_0$)
r_{fr}	Radius of the FR
r_n	Radius of the n-th Fresnel zone
S_i	Area of the FR; $i = 0$ for air, $i = 1$ for air, $i = 2$ for beam, $i = 3$ for ceiling
P_i	Power of the radio wave propagating through the FR; $i = 1$ for air, $i = 2$ for beam, $i = 3$ for ceiling
ϕ_i	Phase of the radio wave propagating through the FR; $i = 1$ for air, $i = 2$ for beam
H_B	Height of beam
W_B	Width of beam
L_B	Length of beam
δ	Thickness of ceiling

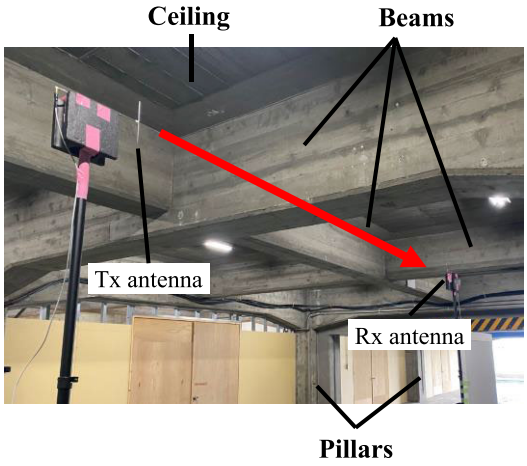

FIGURE 1. Indoor scenario of the ceiling with concrete beams.

II. INDOOR SCENARIOS OF CEILING WITH CONCRETE BEAMS

This chapter describes the indoor scenario addressed in this study. The FDTD simulation results and measurement data are also presented to clarify the path loss characteristics close to a ceiling with a concrete beam.

A. FDTD SIMULATION MODEL

Figure 1 shows a ceiling with concrete beams in a concrete building. As shown in Fig. 1, the concrete pillars and beams on the ceiling are assembled in a grid pattern with no concrete walls near the Tx and Rx antennas. It was reported in [18] that the FDTD simulation results depicted in Fig. 2 are in good agreement with the measured data. The simulation results obtained by the simulation model in Fig. 2 are therefore used in this paper to investigate the propagation path loss.

A beam with a height of $H_B = 0.7$ m, width of $W_B = 0.4$ m, and length of $L_B = 10.0$ m was used for

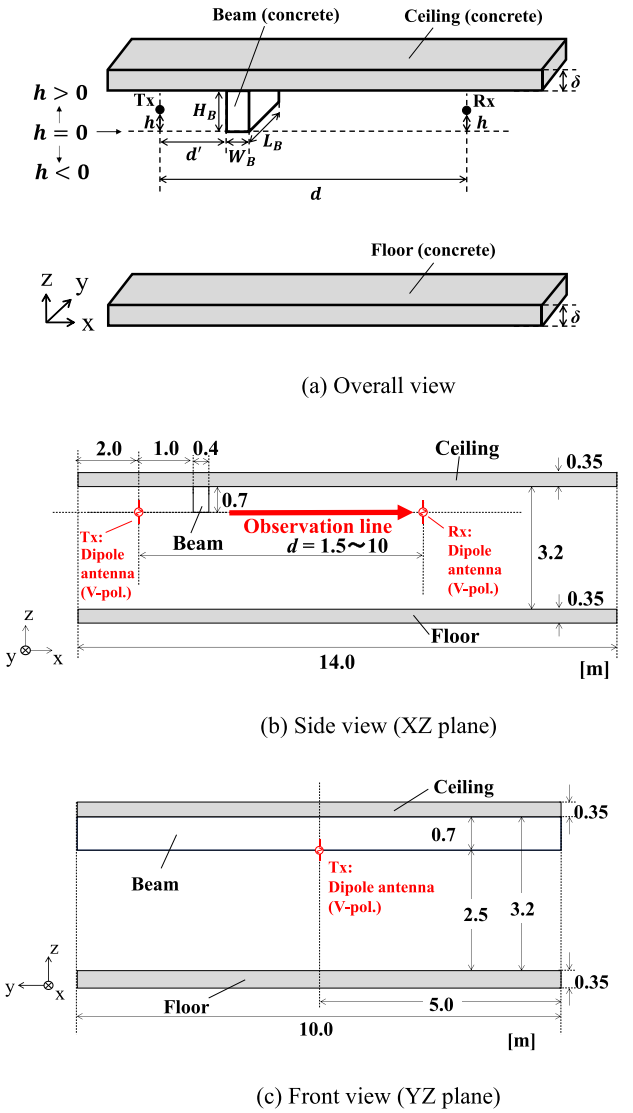

FIGURE 2. FDTD simulation model.

the simulation. Vertically oriented half-wave dipole antennas were employed as the Tx and Rx antennas. The frequency was 928 MHz. The Tx antenna was set at a distance of $d' = 1.0$ m from the surface of the beam in the –x direction, as shown in Fig. 2(a). The Rx antenna was moved along the observation line.

The height h of the Tx and Rx antennas is defined as 0 at the bottom of the beam, $h > 0$ (NLoS) in the +z direction, and $h < 0$ (LoS: line-of-sight situation) in the –z direction.

The path loss L is calculated within the range of $d = 1.5$ - 10 m from the observation line shown in Fig. 2(b) and is defined as follows.

$$L\,[\mathrm{dB}] = P_t\,[\mathrm{dBm}] - P_r\,[\mathrm{dBm}] + G_t\,[\mathrm{dBi}] + G_r\,[\mathrm{dBi}]\,, \quad (1)$$

where P_t is transmitted power, P_r is received power, G_t is Tx antenna gain, and G_r is Rx antenna gain. In this study,

TABLE 2. FDTD simulation parameters [18].

Frequency	928 MHz
Cell size	λ/10
Analysis space	5λ
Wave source	Continuous wave
Boundary condition	PML 8 layer
Convergence judgment condition	0.0001

Parts	Material	Complex relative permittivity
Beam	Concrete	$\varepsilon_r = 5.31 - j0.59$ $\mu_r = 1$
Ceiling		
Floor		
Floor space	Air	$\varepsilon_r = 1$ $\mu_r = 1$

a maximum gain of 2.15 dBi for the dipole antenna was used for G_t and G_r.

B. SIMULATION CONDITIONS

The simulation conditions are summarized in Table 2. The cell size is λ/10, where λ is the wavelength of 928 MHz. The boundary condition is the perfectly matched layer (PML) with eight layers, and the boundary surfaces are set at a position of 5λ from the simulation model to the outside. The complex relative permittivity of the concrete is $\varepsilon_r = 5.31 - j0.59$ [12].

C. SIMULATION AND MEASUREMENT RESULTS

Figures 3(a)-(c) show the FDTD simulation results and measurement data at $h = +0.1$ m, $+0.35$ m, and $+0.6$ m for shallow, middle, and deep NLoS cases, respectively. It is observed from Fig. 3 that the FDTD results are in good agreement with the measurement data. The FDTD simulations are therefore used to investigate the propagation characteristics near the ceiling beam.

According to [18], the path loss can be approximately expressed by the following equation,

$$L\,(d) = \alpha \cdot 10\log_{10} d + \beta\,[\mathrm{dB}]\,, \quad (2)$$

where d is the distance between the Tx and the Rx antennas, α is the path loss exponent, and β is the path loss when $d = 1$ m.

The FDTD simulation results in Fig. 3 show an increase of almost $\alpha = 2$ with respect to distance d. The path loss can therefore be approximated as a regression line by using the least-squares method when α is fixed at 2 in Eq. (2). The regression line and free space path loss are also shown in Fig. 3. It can also be seen in Fig. 3 that β is a function of h. We will discuss this in the next chapter.

III. PROPOSED CALCULATION METHOD

To obtain the path loss closest to the ceiling with the beam, as described in Chapter II, we consider β when $\alpha = 2$

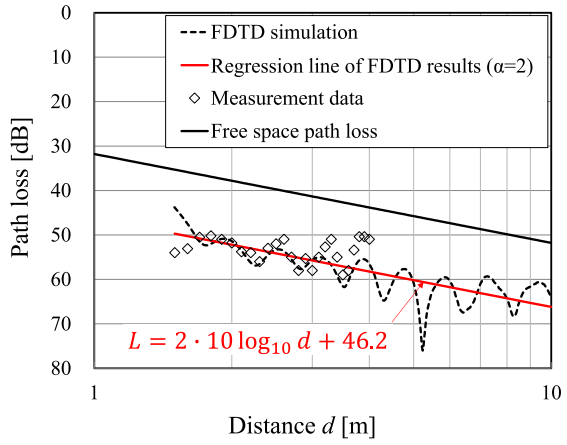

(a) h = +0.1 m

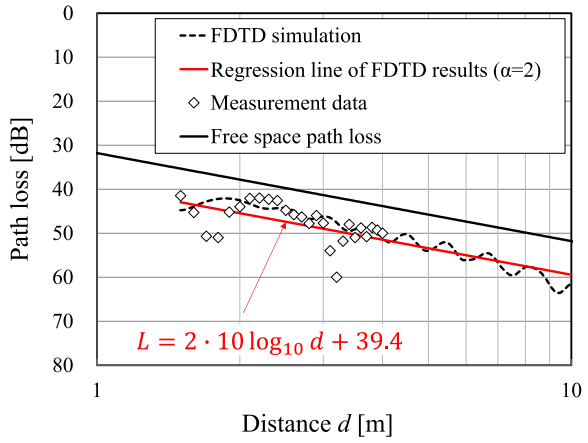

(b) h = +0.35 m

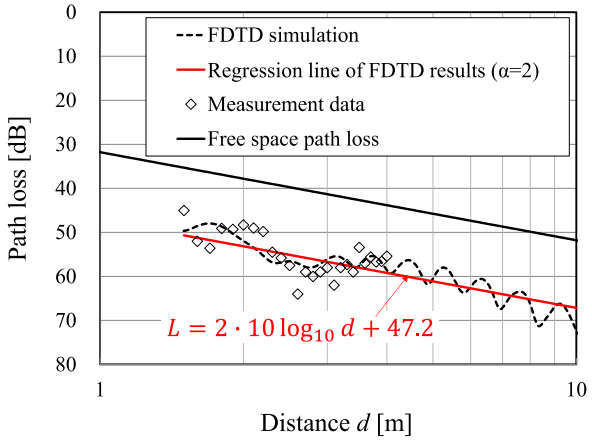

(c) h = +0.6 m

FIGURE 3. FDTD simulation results, regression line where $\alpha = 2$, and measurement data.

in Eq. (1). β is expressed by the following equation,

$$\beta = \beta_0 + \beta_{ex} \ \text{[dB]}, \tag{3}$$

where β_0 is the free space path loss at $d = 1$ m in Eq. (2) and β_{ex} is the excess loss, which is defined as the difference between β and β_0 in dB.

In this chapter, we will attempt to obtain β_{ex} using the forbidden region (FR) technique [19]. The radius r_{fr} of the FR is obtained as 0.6 times that of the first Fresnel zone.

$$r_{fr} = 0.6\, r_1, \tag{4}$$

$$r_n = \sqrt{\frac{n\lambda d_1 d_2}{d_1 + d_2}}, \tag{5}$$

where r_1 is the radius of the first Fresnel zone and λ is the wavelength of the radio wave. d_1 and d_2, respectively, are the distances from the obstruction to the Tx and Rx antennas. Described in detail below are four cases, shown in Figs. 4(a)-(d), with regard to obstruction of the FR by the concrete beam and the concrete ceiling.

Case i: FR is not obstructed by the concrete beam ($h < -r_{fr}$)

In this case, as shown in Fig. 4(a), there are no obstacles in the FR with radius r_{fr}. S_0 and P_0 shown in Fig. 4(a) are the area and radio wave power propagating through the FR. β_{ex} is simply expressed as follows.

$$\beta_{ex} = 0 \ \text{[dB]}. \tag{6}$$

This means that the path loss is equivalent to the free space path loss.

Case ii: FR is partially obstructed by the concrete beam ($-r_{fr} \leq h < r_{fr}$)

In this case, the radio power can be calculated as a combination of two radio waves, one propagating through the air and the other penetrating the concrete beam. Therefore, β_{ex} is expressed as:

$$\beta_{ex} = 10 \log_{10} \frac{P_0}{\left|\sqrt{P_1}\exp(j\phi_1) + \sqrt{P_2}\exp(j\phi_2)\right|^2} \ \text{[dB]}, \tag{7}$$

where P_0 is the power of the radio wave described in Case i, P_1 and ϕ_1 are the power and the phase of the radio wave propagating through the air, respectively, and P_2 and ϕ_2 are the power and phase of the radio wave penetrating the concrete beam. S_1 and S_2 in Fig. 4(b) are areas of the FR of the air and the obstruction of the beams; thus, $S_1 + S_2 = S_0$. P_1 and P_2 are expressed by Eqs. (8) and (9), respectively:

$$P_1 = \left(\frac{S_1}{S_1 + S_2}\right)^2 \times P_0, \tag{8}$$

$$P_2 = \left(\frac{S_2}{S_1 + S_2}\right)^2 \times \frac{1}{L_{concrete}} \times P_0, \tag{9}$$

where $L_{concrete}$ is the transmission loss through the concrete beam.

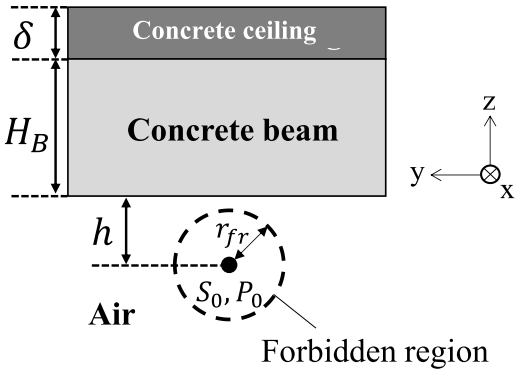

(a) Case i

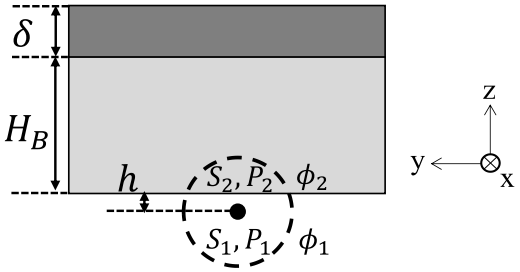

(b) Case ii

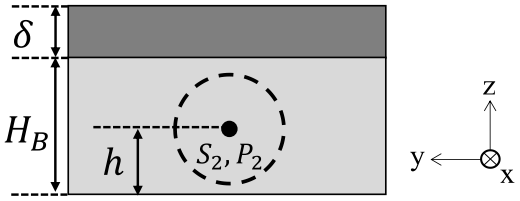

(c) Case iii

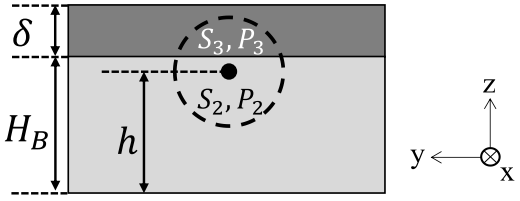

(d) Case iv

FIGURE 4. The positional relationship between the FR and the ceiling with the concrete beam.

ϕ_1 and ϕ_2 in Eq. (7) are obtained by the following equations:

$$\phi_1 = 2\pi \frac{W_B}{\lambda_1} \quad [\text{rad}], \tag{10}$$

$$\phi_2 = 2\pi \frac{W_B}{\lambda_2} \quad [\text{rad}], \tag{11}$$

where W_B is the width of the beam, and λ_1 and λ_2, respectively, are the wavelength of radio waves propagating through the air and the concrete beam. β_{ex} can then be obtained by substituting Eqs. (8)-(11) into Eq. (7).

Case iii: The entire FR is obstructed by the concrete beam ($r_{fr} \leq h \leq H_B - r_{fr}$) In this case, a radio wave penetrates a concrete beam of width $W_B.\beta_{ex}$ is therefore expressed by the following equation using the transmission loss $L_{concrete}$ through the concrete beam:

$$\beta_{\text{ex}} = 10 \log_{10} L_{concrete} \ [\text{dB}]. \tag{12}$$

Case iv: FR is obstructed by concrete beams and ceiling ($H_B - r_{fr} < h$)

Here, r_{fr} is assumed to be less than the thickness δ of the ceiling. P_2 and P_3 in Fig. 4(d) are respectively the power of the radio wave transmitted through the concrete beam and the concrete ceiling. P_3 is assumed to be negligible because the radio wave traveling through the ceiling experiences significant path loss. It can therefore be approximated that $P_3 = 0$. β_{ex} can thus be expressed as:

$$\beta_{ex} = 10 \log_{10} \frac{P_0}{P_2} \ [\text{dB}]. \tag{13}$$

P_2 is expressed by Eq. (14):

$$P_2 = \left(\frac{S_2}{S_2 + S_3} \right)^2 \times \frac{1}{L_{concrete}} \times P_0, \tag{14}$$

where S_2 and S_3 are respectively the area of the concrete beam and the concrete ceiling in the FR.

IV. PATH LOSS PREDICTION USING OUR PROPOSED CALCULATION METHOD

In this chapter, the proposed calculation method is evaluated by comparison with the path loss obtained by the FDTD simulation for the indoor scenario shown in Figure 2.

The evaluation is performed under the conditions of radio frequency of 928 MHz, $d' = 1$ m, $H_B = 0.7$ m, and $\delta = 0.35$ m, as in Figure 2(a).

The radius of FR r_{fr}s of $d = 1.5$ m, 0.2 m, 5 m are respectively 0.2 m, 0.31 m, and 0.32 m, and are obtained using the approximation that a concrete sheet with no width is positioned at the Tx-side surface of the concrete beam. Therefore, a fixed value of $r_{fr} = 0.3$ m, which represents an average value of r_{fr}, is used in this evaluation. The complex relative permittivity of the concrete beams and the ceiling is set at $5.31–j0.59$ [12].

The transmission loss of concrete beam $L_{concrete}$ is calculated using FDTD simulations. Figure 5 illustrates the FDTD simulation model of the concrete wall for calculating $L_{concrete}$. In the model, the length and height of the wall are 10 m, which is sufficiently large with regard to r_{fr} of 0.3 m. The Tx and Rx antennas are placed 1 m from the surface of the wall. The antennas are half-wavelength dipole antennas with vertical polarization.

The boundary surfaces are set at 10λ from the simulation model to the outside. The other simulation conditions are the same as in Table 2. $L_{concrete}$ is obtained by the ratio of the path loss with the wall to that without the wall.

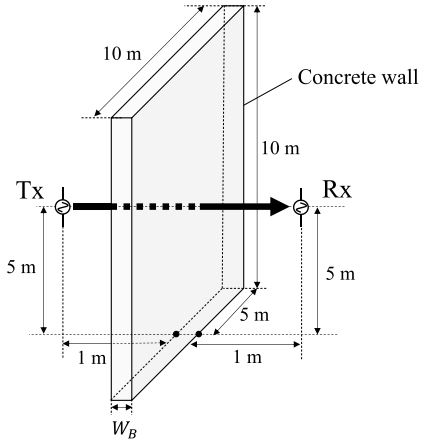

FIGURE 5. FDTD simulation model for calculating $L_{concrete}$.

TABLE 3. Calculated and theoretical values of transmission loss for the thickness of concrete with complex relative permittivity of 5.31-*j* 0.59 [12].

W_B[m]	CALCULATED VALUE $10\log_{10} L_{concrete}$ [dB]	THEORETICAL VALUE $10\log_{10} L_{concrete}$ [dB]
0.3	8.2	8.1
0.4	9.6	10.1
0.5	11.9	12.2

The calculated results of $L_{concrete}$ in dB for changing W_B are listed in Table 3. Table 3 also includes theoretical values of $L_{concrete}$ [6] when plane waves are incident perpendicular to the concrete wall. It is clear that the calculated results agree closely with the theoretical values, thereby confirming by theoretical calculation the effectiveness of the calculation model for $L_{concrete}$ shown in Figure 5. The $L_{concrete}$ calculated by the FDTD simulation was therefore used for the calculation of β_{ex}.

In the next step, β in Eq. (3) is investigated at $\alpha = 2$ by calculating β_{ex} using the proposed calculation method laid out in Chapter III.

Figure 6 shows comparisons of β among the proposed method, FDTD simulation, and measurement data when $h = +0.1$ m, $+0.35$ m, and $+0.6$ m. In Figure 6, the βs of the FDTD simulation and the measurement were obtained as a value at 1 m on a regression line of the data, shown in Fig. 3, when $\alpha = 2$ in Eq. (2).

It is found from Fig. 6 that the maximum difference of β between the FDTD simulation and the measurement is only 1.1 dB. Moreover, the maximum difference of the β between the measurement and the proposed method is 2.4 dB. Thus, the values estimated by the proposed method have an accuracy of this order under these conditions.

Figure 7 shows β as a function of h obtained by FDTD simulation and our proposed calculation method. The figure also shows the regions of Cases i - iv used for the proposed calculation method. Figure 7 shows that the β values obtained by the proposed calculation method are in good agreement with those acquired by FDTD simulation. The difference is within 2.8 dB, indicating that our proposed calculation

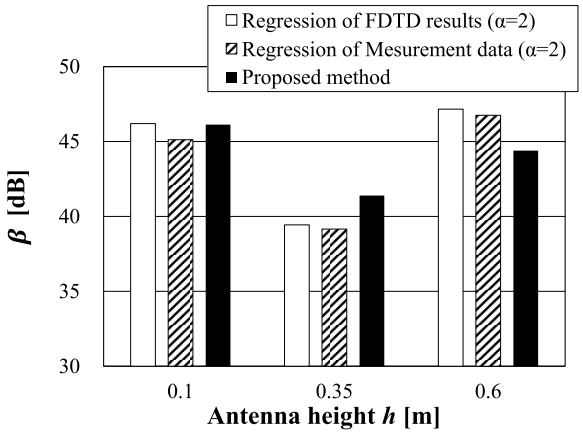

FIGURE 6. Comparison of β among the proposed method, FDTD simulation, and measurement data.

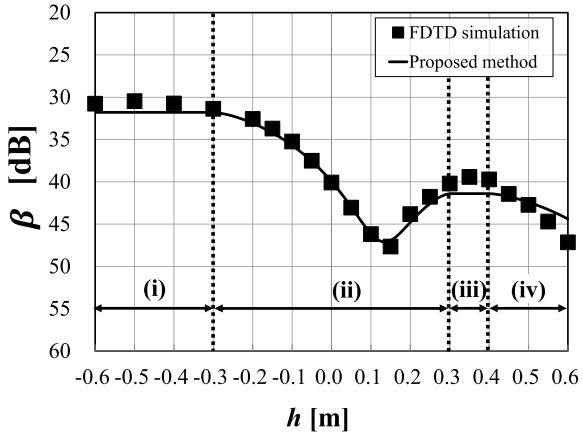

FIGURE 7. β as a function of h obtained by FDTD simulation and the proposed method.

method effectively predicts the path loss close to the ceiling with the concrete beam.

The variation of β in Fig. 7 can be explained using the proposed calculation method. In the Case i region, where the FR is not obstructed by the concrete beam, β is obtained as $\beta_0 = 31.8$ dB at 928 MHz using the Friis Transmission Formula.

In the Case ii region, β is greater than β_0 since the area of the obstruction of the FR by the concrete beam is increased by an increment of h. Moreover, β peaks at $h = 0.14$ m. The concrete beam with $W_B = 0.4$ m and $\varepsilon_r = 5.31 - j0.59$ results in a phase difference of $1.6 \times 2\pi$ radian with respect to air. This means that the radio wave through the air and that through the concrete beam are combined at almost opposite phases. In addition, the amplitudes of P_1 and P_2 in Eqs. (8) and (9) are almost the same at $h = 0.14$ m. β therefore reaches its largest value due to interference between the two waves.

In the Case iii region, where all of the FR is obstructed by the concrete beam, β is a constant value calculated as $31.8 + 9.6 = 41.4$ dB from Eqs. (3) and (12). In the Case iv region, the path loss gradually increases as h increases due to increments in energy loss caused by the obstruction of the ceiling.

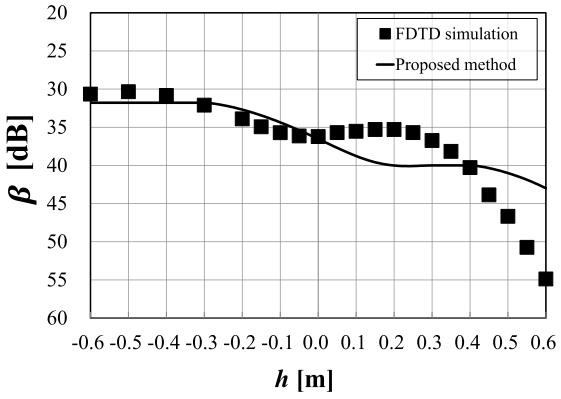

(a) $W_B = 0.3$ m

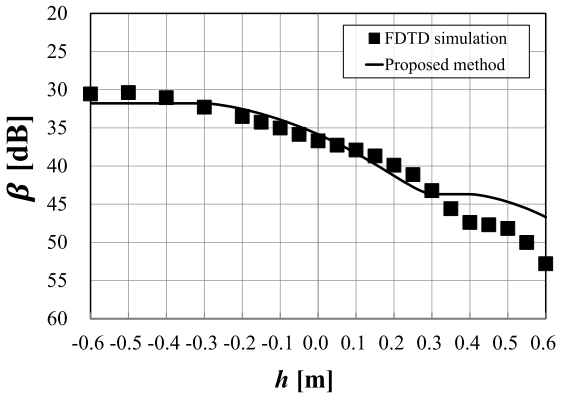

(b) $W_B = 0.5$ m

FIGURE 8. Comparison of β of the concrete beam obtained by FDTD simulation and the proposed calculation method for $W_B = 0.3$ m, 0.5 m, and $\varepsilon_r = 5.31 - j0.59$.

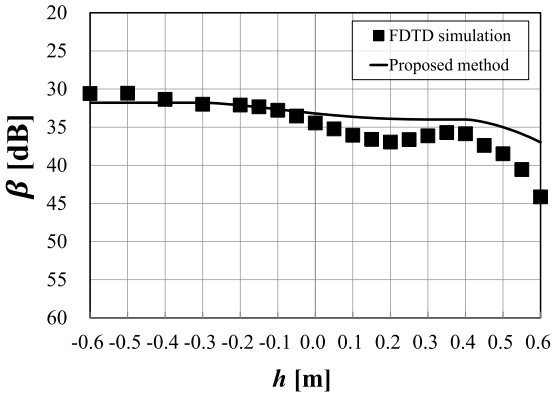

(a) Dry concrete beam ($\varepsilon_r = 3 - j0.1$)

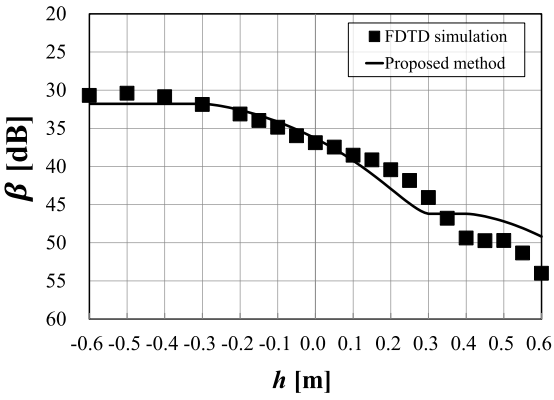

(b) Moist concrete beam ($\varepsilon_r = 7 - j1$)

FIGURE 9. Path losses for the dry and moist concrete beams calculated by FDTD simulation and the proposed calculation method for $W_B = 0.4$ m, $\varepsilon_r = 3 - j0.1$, and $7 - j1$.

V. PATH LOSS PREDICTION UNDER DIFFERENT BEAM CONDITIONS

In this chapter, the path loss β is investigated with different beam widths and different complex relative permittivity values of the concrete, assuming real-world scenario.

Figure 8 shows the path loss characteristics of concrete beams with $W_B = 0.3$ m and 0.5 m, using the calculated value of $L_{concrete}$ in Table 3 for the proposed calculation method. As shown in Fig. 8, the results of the proposed calculation method are in good agreement with that of the FDTD simulation, although there is a large difference that exceeds 5 dB at $h = 0.6$ m. It appears that the approximation of $P_3 = 0$ in the proposed calculation method, shown in Fig. 4(d), causes the difference in path losses in the vicinity of the ceiling surface.

It has been reported that the real and imaginary parts of complex permittivity are positively correlated with the moisture content of the concrete [21], [22], [23]. We therefore evaluated path losses for concrete beams with low and high content with a complex relative permittivity of $3 - j0.1$ and $7 - j1$ [21], [22], [23].

The beam width W_B is 0.4 m, as shown in Fig. 2(a). $L_{concrete}$s for both cases are also calculated by FDTD simulation for the model shown in Figure 5. Table 4 lists the calculated and theoretical values of $L_{concrete}$. In these cases, the calculated results are also in good agreement with the theoretical values.

Figure 9 shows the path loss for the dry and moist concrete beams calculated by FDTD simulation and the proposed calculation method as a function of h. It is evident that the path losses calculated using the proposed method are in good agreement with those of the FDTD simulation. The differences between the path losses using the proposed calculation model and FDTD simulation are also significant at $h = 0.6$ m in the dry and moist cases. Moreover, β of the moist concrete beam is greater than that for dry concrete, especially when h is greater than 0 m. This is because the transmission loss in moist concrete is greater than that in dry concrete, as shown in Table 4. The proposed calculation method is therefore useful for predicting the propagation path loss of a concrete beam on a concrete ceiling.

Finally, the limitation of the application of the proposed method is discussed. The limitation is due to the theory of FR, which is proportional to the first Fresnel zone. From Eqs. (4) and (5), the radius r_{fr} of the FR increases in proportion to the square root of the wavelength λ. This indicates that the r_{fr} increases with decreasing frequency. However, the r_{fr}

TABLE 4. Transmission loss for complex relative permittivity of concrete with a width of $W_B = 0.4$ m.

Concrete condition (Complex relative permittivity ε_r)	Calculated value $10\log_{10} L_{concrete}$ [dB]	Theoretical value $10\log_{10} L_{concrete}$ [dB]
Dry (3-j0.1)	2.2	2.7
Moist (7-j1)	14.4	14.8

needs to be smaller than the distance d_1 and d_2 for obtaining a good approximation to Eq. (5) [19].

In this paper, the minimum values of d_1 and d_2 are 1 m and 0.5 m. The wavelength λ is 0.32 m at 928 MHz. Thus, the radius r_{fr} of the FR is 0.2 m, which is less than d_1 and d_2.

VI. CONCLUSION

In this paper, we propose a simple calculation method for predicting radio propagation path loss in environments that have dielectric obstructions such as a concrete beam between Tx and Rx.

First, the propagation path loss characteristics near the concrete ceiling beam at 928 MHz were shown by FDTD simulation and measurement in an actual concrete building. The calculation accuracy of the FDTD simulation was also evaluated in comparison with the measured data. The details of a simple calculation method based on the theory of the forbidden region were then explained. The effectiveness of the proposed method was verified by comparison between the FDTD simulation results and the measurements. The results indicated the proposed method to be in good agreement (within 2.8 dB) with the FDTD simulation results. Our proposed method agrees fairly well with the FDTD simulation results for a variety of structural and material conditions of concrete beams.

The limitation of application of the proposed method was also discussed. We concluded that our proposed method can be used in spite of the frequency limitations caused by the approximation used to obtain the radius of the FR.

In conclusion, a prediction method of a propagation path loss with a radio wave passing through a dielectric material was successfully formulated that is applicable to indoor IoT wireless communications.

In future work, the applicability of the proposed method at higher frequencies, such as in the 2.4 GHz, 5 GHz and 6 GHz bands, will be investigated.

REFERENCES

[1] S. Al-Sarawi, M. Anbar, R. Abdullah, and A. B. A. Hawari, "Internet of Things market analysis forecasts, 2020–2030," in *Proc. 4th World Conf. Smart Trends Syst., Secur. Sustainability (WorldS4)*, Jul. 2020, pp. 449–453, doi: 10.1109/WorldS450073.2020.9210375.

[2] H. A. H. Alobaidy, M. J. Singh, M. Behjati, R. Nordin, and N. F. Abdullah, "Wireless transmissions, propagation and channel modelling for IoT technologies: Applications and challenges," *IEEE Access*, vol. 10, pp. 24095–24131, 2022, doi: 10.1109/ACCESS.2022.3151967.

[3] H. Xia, H. L. Bertoni, L. R. Maciel, A. Lindsay-Stewart, and R. Rowe, "Radio propagation characteristics for line-of-sight microcellular and personal communications," *IEEE Trans. Antennas Propag.*, vol. 41, no. 10, pp. 1439–1447, Oct. 1993, doi: 10.1109/8.247785.

[4] M. J. Feuerstein, K. L. Blackard, T. S. Rappaport, S. Y. Seidel, and H. H. Xia, "Path loss, delay spread, and outage models as functions of antenna height for microcellular system design," *IEEE Trans. Veh. Technol.*, vol. 43, no. 3, pp. 487–498, Aug. 1994, doi: 10.1109/25.312809.

[5] *Propagation by Diffraction*, document ITU-R P.526-15, 2019.

[6] M. Born and E. Wolf, *Principles of Optics: Electromagnetic Theory of Propagation, Interference and Diffraction of Light*, 7th ed. Cambridge, U.K.: Cambridge Univ. Press, 1999, doi: 10.1017/cbo9781139644181.

[7] J. B. Keller, "Geometrical theory of diffraction," *J. Opt. Soc. Amer.*, vol. 52, no. 2, pp. 116–130, 1962, doi: 10.1364/JOSA.52.000116.

[8] R. Luebbers, "Finite conductivity uniform GTD versus knife edge diffraction in prediction of propagation path loss," *IEEE Trans. Antennas Propag.*, vol. AP-32, no. 1, pp. 70–76, Jan. 1984, doi: 10.1109/TAP.1984.1143189.

[9] R. G. Kouyoumjian and P. H. Pathak, "A uniform geometrical theory of diffraction for an edge in a perfectly conducting surface," *Proc. IEEE*, vol. 62, no. 11, pp. 1448–1461, Nov. 1974, doi: 10.1109/PROC.1974.9651.

[10] P. D. Holm, "A new heuristic UTD diffraction coefficient for nonperfectly conducting wedges," *IEEE Trans. Antennas Propag.*, vol. 48, no. 8, pp. 1211–1219, Aug. 2000, doi: 10.1109/8.884489.

[11] R. J. Luebbers, "A heuristic UTD slope diffraction coefficient for rough lossy wedges," *IEEE Trans. Antennas Propag.*, vol. 37, no. 2, pp. 206–211, Feb. 1989, doi: 10.1109/8.18707.

[12] *Effects of Building Materials and Structures on Radiowave Propagation Above About 100 MHz*, document document ITU-R P.2040-1, 2015.

[13] Y. Kishiki and J. Takada, "Improvement of 3D ray tracing simulation in microcell environment by introducing the complex radar cross section," in *Proc. Int. Symp. Antennas Propag. (ISAP)*, Taiwan, Oct. 2008, pp. 790–793, doi: 10.34385/proc.35.2A02-4.

[14] V. Degli-Esposti, D. Guiducci, A. de'Marsi, P. Azzi, and F. Fuschini, "An advanced field prediction model including diffuse scattering," *IEEE Trans. Antennas Propag.*, vol. 52, no. 7, pp. 1717–1728, Jul. 2004, doi: 10.1109/TAP.2004.831299.

[15] K. Yee, "Numerical solution of initial boundary value problems involving Maxwell's equations in isotropic media," *IEEE Trans. Antennas Propag.*, vol. AP-14, no. 3, pp. 302–307, May 1966, doi: 10.1109/TAP.1966.1138693.

[16] Y. Suzuki and M. Omiya, "Computer simulations for a site-specific modeling of indoor radio wave propagation," in *Proc. IEEE Region 10 Conf. (TENCON)*, Singapore, Nov. 2016, pp. 123–126, doi: 10.1109/TENCON.2016.7847972.

[17] A. C. M. Austin, M. J. Neve, and G. B. Rowe, "Modeling propagation in multifloor buildings using the FDTD method," *IEEE Trans. Antennas Propag.*, vol. 59, no. 11, pp. 4239–4246, Nov. 2011, doi: 10.1109/TAP.2011.2164181.

[18] N. Yamamoto, T. Sasaki, A. Yamamoto, T. Hishikawa, K. Saito, J.-I. Takada, and T. Maeyama, "920 MHz path loss prediction formula based on FDTD method for IoT wireless system close to ceiling with concrete beam," *IEICE Trans. Commun.*, vol. E105.B, no. 12, pp. 1540–1547, Dec. 2022, doi: 10.1587/transcom.2022EBP3010.

[19] S. R. Saunders and A. Aragón-Zavala, *Antennas and Propagation for Wireless Communication Systems*, 2nd ed. Hoboken, NJ, USA: Wiley 2007.

[20] K. Mochizuki, K. Obata, K. Mizutani, and H. Harada, "Development and field experiment of wide area Wi-SUN system based on IEEE 802.15.4g," in *Proc. IEEE 3rd World Forum Internet Things (WF-IoT)*, Reston, VA, USA, Dec. 2016, pp. 76–81, doi: 10.1109/WF-IoT.2016.7845425.

[21] M.-K. Olkkonen, V. Mikhnev, and E. Huuskonen-Snicker, "Complex permittivity of concrete in the frequency range 0.8 to 12 GHz," in *Proc. 7th Eur. Conf. Antennas Propag. (EuCAP)*, Gothenburg, Sweden, Apr. 2013, pp. 3319–3321.

[22] G. Villain, A. Ihamouten, and X. Dérobert, "Use of frequency power law to link the results of two EM testing methods for the characterization of humid concretes," in *Proc. 6th Int. Workshop Adv. Ground Penetrating Radar (IWAGPR)*, Aachen, Germany, Jun. 2011, pp. 1–5, doi: 10.1109/IWAGPR.2011.5963901.

[23] H. Chiba and Y. Miyazaki, "Analysis of radio wave reflection and transmission characteristics at reinforced concrete slab by numerical simulation and scaled model experiment," in *Proc. Int. Symp. Electromagn. Compat.*, Tokyo, Japan, 1999, pp. 424–427, doi: 10.1109/ELMAGC.1999.801355.

NAOTAKE YAMAMOTO (Member, IEEE) received the B.S. and M.S. degrees in electrical engineering from the Tokyo University of Science, Japan, in 2001 and 2003, respectively. He joined Panasonic Corporation, (the former Matsushita Electric Industrial Company Ltd.), Osaka, in 2003, where his work included developing wireless systems, such as intercommunication systems, home energy management systems, lighting systems, and ventilation systems. His research interests include antennas and radio propagation. He is a member of IEICE.

TAICHI SASAKI (Member, IEEE) received the B.S. and M.S. degrees from Kyoto University, in 2018 and 2020, respectively. In 2020, he joined Panasonic Corporation, Osaka, Japan, and he has been engaged in research and development of antennas and the propagation of wireless communications.

ATSUSHI YAMAMOTO received the B.S. and M.S. degrees from Okayama University, in 1995 and 1997, respectively. In 1997, he joined Matsushita Electric Industrial Company Ltd. (Panasonic Corporation), Osaka, Japan, and he has been engaged in research and development of antennas and the propagation of wireless communications. He is a member of IEICE.

TETSUYA HISHIKAWA received the Associate degree in electrical engineering from the National Institute of Technology, Gifu College, in 1986. He joined Panasonic Corporation (the former Matsushita Electric Industrial Company Ltd.), Osaka, in 1986, and he has been engaged in the research and development of wireless communication systems products, such as mobile communication base stations and various wireless applications.

JUN-ICHI TAKADA (Senior Member, IEEE) received the B.E., M.E., and D.E. degrees in electrical and electronic engineering from the Tokyo Institute of Technology, Tokyo, Japan, in 1987, 1989, and 1992, respectively.

He was a Research Associate with Chiba University, Chiba, Japan, from 1992 to 1994, and an Associate Professor with the Tokyo Institute of Technology, from 1994 to 2006, where he has been a Professor, since 2006. He was also a Researcher with the National Institute of Information and Communications Technology, Kanagawa, Japan, from 2003 to 2007. His research interests include radio-wave propagation and channel modeling for mobile and short-range wireless systems, regulatory issues in relation to spectrum sharing, and ICT applications for international development.